Accepted Manuscript

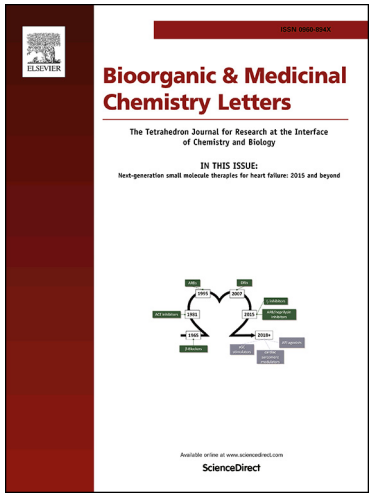

Development and characterization of a CNS-penetrant benzhydryl hydroxamic acid class IIa histone deacetylase inhibitor

Christopher A. Luckhurst, Omar Aziz, Vahri Beaumont, Roland W. Bürli, Perla Breccia, Michel C. Maillard, Alan F. Haughan, Marieke Lamers, Phil Leonard, Kim L. Matthews, Gilles Raphy, Andrew J. Stott, Ignacio Munoz-Sanjuan, Beth Thomas, Michael Wall, Grant Wishart, Dawn Yates, Celia Dominguez

PII: S0960-894X(18)30858-8
DOI: https://doi.org/10.1016/j.bmcl.2018.11.009
Reference: BMCL 26120

To appear in: *Bioorganic & Medicinal Chemistry Letters*

Received Date: 14 August 2018
Revised Date: 2 November 2018
Accepted Date: 5 November 2018

Please cite this article as: Luckhurst, C.A., Aziz, O., Beaumont, V., Bürli, R.W., Breccia, P., Maillard, M.C., Haughan, A.F., Lamers, M., Leonard, P., Matthews, K.L., Raphy, G., Stott, A.J., Munoz-Sanjuan, I., Thomas, B., Wall, M., Wishart, G., Yates, D., Dominguez, C., Development and characterization of a CNS-penetrant benzhydryl hydroxamic acid class IIa histone deacetylase inhibitor, *Bioorganic & Medicinal Chemistry Letters* (2018), doi: https://doi.org/10.1016/j.bmcl.2018.11.009

Bioorganic & Medicinal Chemistry Letters
journal homepage: www.elsevier.com

Development and characterization of a CNS-penetrant benzhydryl hydroxamic acid class IIa histone deacetylase inhibitor.

Christopher A. Luckhurst[a], Omar Aziz[a], Vahri Beaumont[b], Roland W. Bürli[a], Perla Breccia[a], Michel C. Maillard[b,*], Alan F. Haughan[a], Marieke Lamers[a], Phil Leonard[a], Kim L. Matthews[a], Gilles Raphy[a], Andrew J. Stott,[a] Ignacio Munoz-Sanjuan[b], Beth Thomas[a], Michael Wall[a], Grant Wishart[a], Dawn Yates[a] and Celia Dominguez[b].

[a] *Charles River Discovery (previously BioFocus), Chesterford Research Park, Saffron Walden, Essex, CB10 1XL, United Kingdom*
[b] *CHDI Management/CHDI Foundation Inc., 6080 Center Drive, Suite 700, Los Angeles, California 90045, United States*

ARTICLE INFO

Article history:
Received
Revised
Accepted
Available online

Keywords:
CHDI-390576
Hydroxamic acid
CNS-penetrant
HDAC4 inhibition
Class IIa HDAC inhibitor

ABSTRACT

We have identified a potent, cell permeable and CNS penetrant class IIa histone deacetylase (HDAC) inhibitor **22**, with >500-fold selectivity over class I HDACs (1,2,3) and ~150-fold selectivity over HDAC8 and the class IIb HDAC6 isoform. Dose escalation pharmacokinetic analysis demonstrated that upon oral administration, compound **22** can reach exposure levels in mouse plasma, muscle and brain in excess of cellular class IIa HDAC IC_{50} levels for ~ 8 h. Given the interest in aberrant class IIa HDAC function for a number of neurodegenerative, neuromuscular, cardiac and oncology indications, compound **22** (also known as CHDI-390576) provides a selective and potent compound to query the role of class IIa HDAC biology, and the impact of class IIa catalytic site occupancy *in vitro* and *in vivo*.

* Corresponding author. Tel.: +1-310-342-5506; fax: +1-310-342-5519; e-mail: Michel.Maillard@chdifoundation.org

Class IIa histone deacetylases (HDAC) are classically described as transcriptional corepressor enzymes that interact with MEF2 transcription factors and the N-CoR, BCoR, and CtBP corepressors[1-4]. They are distinct from class I and IIb HDACs in that they bind to, but do not remove, acetylated lysines due to their low catalytic activity [2, 5, 6] and are capable of shuttling between the cytoplasm and nucleus, hence they are directly linked to cellular signaling networks. Class IIa HDACs have been implicated in a wide variety of biological processes, playing key roles in activity-dependent gene regulation in response to neural activity both in the CNS, heart, and at the neuromuscular junction[2, 7]. In particular, the therapeutic potential of HDAC4 inhibition has been proposed as a therapeutic strategy to combat such diverse indications as inflammatory hyperalgesia [8] cardiac hypertrophy [6, 9], certain cancers [10, 11], muscle-wasting disorders [12-14], and has therapeutic potential in progressive neurodegenerative diseases such as amyotrophic lateral sclerosis (ALS)[15-17], and Huntington's disease [3, 18]. However, an outstanding question for the field is how occupancy of the acetyl-binding site of class IIa HDACs with drugs affects class IIa HDAC signaling, and whether this could confer some or all of the same benefits as genetic suppression of HDAC4 expression in these diverse disease indications.

We previously reported the design, synthesis and profiling of cyclopropane hydroxamic acids [19, 20] (**Figure 1**) to evaluate the effect of occupancy of the class IIa HDAC lysine-binding domain on class IIa activity. We now describe the optimization of benzhydryl hydroxamic acids with improved CNS properties and HDAC class IIa selectivity.

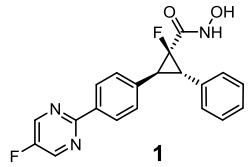

1

Figure 1. Cyclopropane hydroxamic acid **1**.

Hydroxamic acids **2** and **3** (**Table 1**) [21] showed biochemical class IIa HDAC (4, 5, 7, 9) selectivity over class I (HDAC3, 8) and IIb (HDAC6) isoforms, with micromolar inhibition of class IIa enzymes in a cellular context, and no activity up to 50 μM with the "Lys-Ac class I/IIb specific" cell assay (see Supplemental Methods for assay conditions).

Table 1. Biochemical and cell selectivity data for benzhydryl and fluorene hydroxamic acid HDAC inhibitors.

Compound		**2**	**3**
Structure		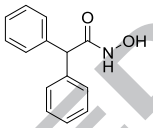	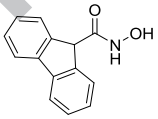
Biochemical IC_{50}	HDAC4	0.25	0.33
	HDAC5	0.16	0.15
	HDAC7	0.65	0.07
	HDAC9	0.51	0.12
	HDAC3	>50	38.9
	HDAC8	43.0	15.5
	HDAC6	11.0	4.9
Cell (Jurkat) IC_{50} (Lys substrate)	TFA	2.9	0.77
	Ac	>50	>50

[a] Inhibition IC_{50} values in μM. Geometric mean and standard deviation <25% of the mean. Assay conditions are described in the Supplemental Information, section 3: supplemental materials & methods.

Early in the program, capping of the phenylene linker of benzhydryl scaffold **2** was investigated towards improving potency (see **Table 2** for nomenclature of compound regions). Efforts were focused on the *para* position of the phenylene linker where docking studies suggested a further pi-stacking interaction could be exploited with HDAC4 residue Phe871 (*vide infra*). Initially, inhibitors of HDAC class IIa enzymes with peripherally-restricted exposures were investigated with sulfonanilide derivatives (**Table 2**), given the high expression of HDAC4 in muscle and heart, and the implication that block of HDAC4 activity could be beneficial in some neuromuscular and cardiac pathologies[10, 11, 15]. Compound **4** displayed good HDAC4 biochemical (22 nM) and cell activity (38 nM), with ligand efficiency of 0.37. The 2-fluorophenyl lower pocket moiety conferred *ca*. 3-fold improvement in cellular activity over the unsubstituted phenyl and other fluorophenyl isomers. Compounds in this series, with high topological polar surface area (TPSA) and an additional hydrogen bond donor to the hydroxamic acid, demonstrated high P-gp efflux, and poor passive permeability in wild-type MDCK cell monolayers. Upon oral dosing of compound **4** in mice, poor bioavailability (8%) and negligible brain exposure were observed.

Table 2. *In vitro* properties for sulfonanilide hydroxamic acid **4**, showing general nomenclature of compound regions.

Compound **4**	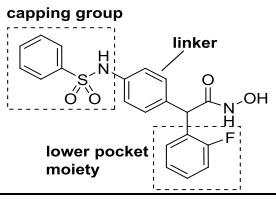
HDAC4 IC_{50}[a]	0.022
Cell IC_{50}[a] Lys-TFA	0.038
Cell IC_{50}[a] Lys-Ac	>50
MDCK-MDR1: EER[b]	47
MDCK WT P_{app} (nm/s)	32
Kinetic solubility (μM)	187
TPSA (Å^2)	96
AlogP	3.0

[a] Inhibition IC_{50} values in μM. Geometric mean and standard deviation <25% of the mean; [b] An effective efflux ratio (EER: B to A/A to B ratio) value of >4 suggests that a compound is a substrate for P-gp, whereas values <2 suggest the compound is unlikely to be a P-gp substrate. For delivery to the CNS, a drug candidate should ideally have an *in vitro* passive permeability >150 nm/s and an EER < 2[22]

Methylation of the sulfonanilide NH conferred no reduction in P-gp efflux (high effective efflux (EER) ratio) nor improvement in passive permeability in wild-type MDCK cell monolayers. In addition, reduction in cellular activity was also observed. The derivative of compound **4** with a 2-pyridyl linker showed much reduced activity in the HDAC4 biochemical assay (HDAC4 IC_{50} 2.2 μM; cell IC_{50} 6.4 μM). With the linker and sulfonamide changes not delivering on potency and *in vitro* properties, we focused our efforts towards the introduction of alternative capping groups with a phenylene linker.

New capping group moieties were sought to achieve physicochemical properties suitable to deliver improved bioavailability and CNS exposure, and most encouraging results were seen for compounds comprising heteroaromatic capping groups directly appended to the phenylene linker. During the development of CNS-penetrant class IIa HDAC inhibitors it was confirmed that molecules with the 2-fluorophenyl lower pocket moiety displayed improved cellular activities *versus* their unsubstituted phenyl ring counterparts, albeit with similar HDAC4 biochemical values. Consistent with this improvement in cellular activity, the additional 2-fluoro moiety may be acting as a hydrogen bond acceptor, its proximity to the hydroxamic acid moderating the NH hydrogen bond donor. Nitrogen-containing heterocycles were not tolerated in this position (data not shown).

Attention was paid to limiting TPSA and the number of hydrogen bond donors throughout the design of these molecules (**Table 3**). Compounds with a heteroaryl capping group in the *para* position of the phenylene linker were significantly more active in the biochemical and cellular assays than those with a *meta* capping group, suggesting better occupancy of the channel bounded by Phe871 for the *para*-capping group molecules. Compound **5**, with a 4-pyridyl capping group, exhibited moderate cell potency (410 nM). Other heterocycles **6-12** displayed improved cell activity. Compound **7** showed moderate Cl_{int} in mouse microsomes, but high P-gp efflux and low passive permeability in wild-type MDCK cells.

Following an oral dose in mice, **7** (**Table 3**) demonstrated very low total brain exposure and poor bioavailability (11%). Other compounds (**6**, **8**-**10**) with heterocyclic capping groups generally displayed high P-gp efflux. Oxazole **12**, with good cell potency, moderate microsomal stability, and notably lower P-gp efflux, demonstrated some improvement in brain exposure and oral bioavailability (39%, data not shown).

Table 3. Heterocyclic capping groups and their impact on P-gp efflux, passive permeability and microsomal clearance.

Compound	**5**	**6**	**7**	**8**	**9**	**10**	**11**	**12**
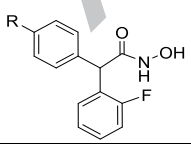								
HDAC4 IC_{50}[a]	0.103	0.033	0.031	0.022	0.040	0.030	0.022	0.025
Cell IC_{50}[a] Lys-TFA	0.410	0.088	0.108	0.091	0.059	0.138	0.127	0.079
Cell IC_{50}[a] Lys-Ac	>50	>50	>50	>50	>50	>50	>50	>50
MDCK-MDR1: EER[b]	-	5.9	6.9	2.9	3.7	6.9	2.5	1.8
MDCK WT P_{app} (nm/s)	-	110	67	326	464	40	431	403
Mouse microsome Cl_{int}[c]	-	168	77	138	391	<65	300	111
Kinetic solubility (μM)	-	138	173	175	164	191	192	118
TPSA (Å^2)	62	75	75	75	75	67	62	76

AlogP	2.7	2.9	2.5	2.8	2.2	2.6	2.9	2.3

[a] Inhibition IC_{50} values in μM. Geometric mean and standard deviation <25% of the mean; [b] See footnote for **Table 2**; [c] Intrinsic clearance (Cl_{int}) values of > 257 mL/min/kg in mouse liver microsomes (MLM) indicate a rapid rate of oxidative metabolism. Under the assay conditions used Cl_{int} values < 65 mL/min/kg in MLM indicate low rate of metabolism by CYP450 enzymes.

Structure-activity studies were undertaken with a subseries of compounds containing a pyrimidinyl capping group (**Table 4**). Compounds with a 5-pyrimidinyl moiety (examples **15-18**) generally displayed good cellular activity (< 150 nM), moderate stability in mouse microsomes, and EER values between 3 and 4 (predicting moderate P-gp efflux).

The 2-pyrimidinyl compounds **19-23** were slightly more active in the cellular assay and displayed significantly reduced P-gp efflux than their 5-pyrimidinyl counterparts **15-18**. Unsubstituted pyrimidine **19** and the *para*-methylated derivative **21** were both unstable in mouse microsomes, whilst *para*-fluoro analog **20** showed an improvement in microsomal stability. 5-Trifluoromethyl-pyrimidin-2-yl compound **22** was more active in the HDAC4 and cellular assays than the 4-trifluoromethyl pyrimidin-2-yl analog **23**, and the former was also more stable in mouse microsomes.

Compounds **16** and **22** were similar in their *in vitro* properties, such as mouse microsomal stability, kinetic aqueous solubility, with a small difference in cell activity. The only notable difference between these two compounds was in the potential for P-gp-mediated efflux. With MDCK-MDR1 EER values for **16** and **22** of 3.0 and 1.2 respectively, it remained to be seen what effect, if any, this might have upon brain exposure *in vivo*.

Compound **22** was synthesized according to the route shown in **Scheme 1**. Addition of 2-fluorobenzaldehyde to the Grignard reagent furnished the benzhydryl alcohol, which was converted to the chloride. Cyanide displacement followed by acid-mediated methanolysis provided the methyl ester. Formation of the cyclic boronate ester from the aryl bromide followed by Suzuki coupling of bromopyrimidine and subsequent treatment with basic aqueous hydroxylamine gave compound **22**.

Table 4. Pyrimidine capping group regiochemistry and substituent effects.

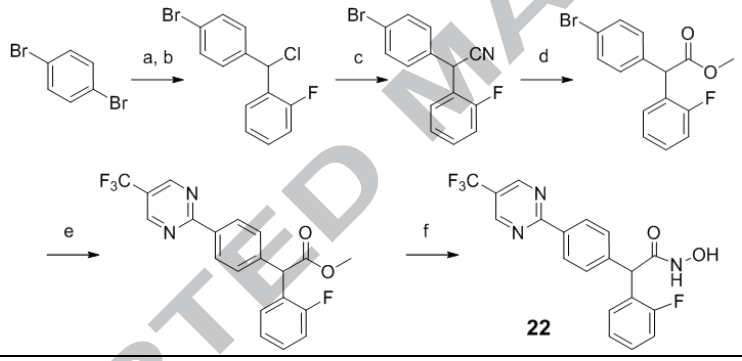

22

Compound	**15**	**16**	**17**	**18**	**19**	**20**	**21**	**22**	**23**
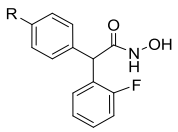								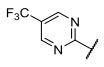	
HDAC4 IC_{50}[a]	0.057	0.039	0.055	0.049	0.025	0.025	0.017	0.054	0.119
Cell IC_{50}[a] Lys-TFA	0.130	0.127	0.108	0.154	0.072	0.057	0.032	0.069	0.128
Lys-Ac	>50	>50	>50	>50	>50	>50	>50	>50	>50
MDCK-MDR1: EER[b]	5.9	3.0	4.1	3.0	1.1	1.6	NV[d]	1.2	NV[d]
MDCK WT P_{app} (nm/s)	268	280	352	159	351	438	NV[d]	294	NV[d]
Mouse microsome Cl_{int}[c]	72	79	135	144	>1297	235	>1297	73	170
Kinetic solubility (μM)	>200	186	140	190	16	<5	52	143	141
TPSA (Å^2)	75	75	75	75	75	75	75	75	75
AlogP	2.3	2.4	3.0	2.6	2.4	2.6	2.9	3.2	3.1

[a] Inhibition IC_{50} values in μM. Geometric mean and standard deviation <25% of the mean; [b] See footnote for **Table 2**; [c] Intrinsic clearance (Cl_{int}), see footnote for **Table 3**; [d] NV = no value: data could not be generated due to Lucifer yellow fails, which may indicate that the test compound is cytotoxic.

Scheme 1. Synthesis of trifluoromethyl pyrimidine **22**. Reagents and conditions: (a) Mg, Et_2O; 2-fluorobenzaldehyde, (55% yield); (b) $SOCl_2$, DCM, r.t., (94%); (c) TMSCN, $TiCl_4$, DCM, r.t., (99%); (d) MeOH, conc. H_2SO_4, reflux, (63%); (e) i) *bis*-(pinacolato)diboron, CsF, $Pd(PPh_3)_4$, DME, MeOH, 1 h, 100 ˚C; ii) 2-chloro-5-trifluoromethylpyrimidine, K_2CO_3, $Pd(PPh_3)_4$, dioxane, water, 100 ˚C, 16 h (60%); (f) 50% aq. hydroxylamine, 15% w/v NaOH, MeOH (82%).

To observe the key interactions with HDAC4, we obtained a co-crystal structure of 2-methyl pyrimidin-5-yl **16** complexed to the catalytic domain of wild type human HDAC4 (**Figure 2**; see Supplemental Methods for protein production and crystallization conditions). This structure crystallized in the space group $P3_2$ with 3 molecules per asymmetric unit (data not shown).

As we previously reported with the cyclopropane hydroxamic acid HDAC4 structures[19, 20] the protein adopted a closed-loop conformation. The ligand binding site formed part of a packing interface in which residue Leu728 of a neighboring HDAC4 chain was positioned close to the ligand. With amino acids 729 to 760 not visible in the electron density maps for any of the 3 molecules in the asymmetric unit this disordered region was removed from the model. Despite being unable to study the interaction between the ligand and residue Asp759, this was still deemed suitable for analysis of the binding mode of the molecule in the active site.

Figure 2. Co-crystal X-ray structure of pyrimidine hydroxamic acid **16** at 2.1 Å resolution (PDB code 6FYZ).

The results from more extensive *in vitro* profiling of compounds **16** and **22** are shown in **Table 5**. Both **16** and **22** potently inhibited HDAC4 with IC_{50} values of 36 and 54 nM, respectively. The affinity (K_d) and binding rate constants (k_{on} and k_{off}) of **16** and **22** to the catalytic domain of immobilized HDAC4 was also determined by surface plasmon resonance technology (**Table S1**). The K_d values were in good agreement with biochemical IC_{50} for each compound. Overall, the two compounds had similar potency across all class IIa HDAC isoforms, with excellent selectivity over the class I HDACs (1, 2, 3) and ~150-fold selectivity over HDAC8 and the class IIb HDAC6 isoform. Compound **22** showed a ~2-fold improvement in class IIa cellular IC_{50} compared to compound **16,** with neither compound showing observable class I/IIb cellular activity up to 50 µM *in vitro* using Boc-Lys-Ac as the exogenous substrate. In A549 cells, compound **22** was evaluated for activity against canonical class I and class IIb substrates histone H4K12 site and tubulin respectively. Class I activity was not observable, and class IIb activity (tubulin acetylation) returned an IC_{50} of 17 µM. Additionally, at a test concentration of 10 µM, both compounds exhibited a 'clean' profile of <25% displacement of selective radioligands against an extensive panel of CNS and peripheral receptors, ion channels, enzymes and transporters (Cerep Diversity panel; data not shown). We conclude that compounds **16** and **22** represent excellent tool compounds to assess the impact of class IIa HDAC catalytic site inhibition or occupancy in a cellular *in vitro* context.

Compounds **16** and **22** both showed approximately equal distribution into mouse blood and plasma. From *in vitro* tissue equilibrium dialysis, the unbound fractions of **16** in plasma (11%) and mouse brain homogenate (12%) were higher than for **22** (4.1% and 0.5% respectively). Both compounds showed no inhibition against CYP450 isoforms (CYPs 1A2, 2C8, 2C9, 2C19, 2D6, 3A4) tested at 50 µM (**16**: CYP3A4 > 35 µM), showed no HERG liability, and no potential genetic toxicity (Ames test negative: Cerep). Compound **22** was stable in mouse and human plasma and blood, and simulated gastric fluid.

Compounds **16** and **22** were progressed *in vivo* to compare their brain exposures given their difference in P-gp efflux values. Following intravenous (5 mg/kg) and oral gavage (10 mg/kg) dosing to fed male C57Bl/6 mice, **16** and **22** were rapidly absorbed and displayed oral bioavailability values of 32% and 44%, respectively (**Table S2** and **S3**). Their PK profiles following oral gavage showing total exposure in plasma, muscle and brain are shown in **Figure 3**. Compound **22** demonstrated a higher volume of distribution (7.3 L/kg) than **16** (1.1 L/kg); as expected, **22** also exhibited a higher distribution of total drug to brain tissue than **16** (**Table S4**), consistent with the estimated lower P-gp substrate liability of compound **22** *versus* that of **16**. When plasma protein and brain tissue binding were taken into account, the unbound brain-to-plasma partition ratios ($Kp_{uu,brain}$) for **16** and **22** were similar at C_{max} (0.12 and 0.14 respectively). Compound **16** displayed high plasma clearance *in vivo* (6.4 L/h/kg) which was moderately improved in **22** (3.1 L/h/kg); *in vitro* mouse hepatocyte Cl_{int} values were high for both **16** and **22** at 264 and 383 mL/min/kg body weight respectively, with direct *O*-glucuronidation of the hydroxamic acid a likely metabolic fate for these molecules (not shown).

Table 5. *In vitro* profiles of pyrimidines **16** and **22**.

Assay		Substrate	**16**	**22**
Biochemical IC_{50} (µM) [a]	HDAC4	Boc Lys(TFA)	0.036	0.054
	HDAC5	Boc Lys(TFA)	0.016	0.060
	HDAC7	Boc Lys(TFA)	0.023	0.031
	HDAC9	Boc Lys(TFA)	0.030	0.050

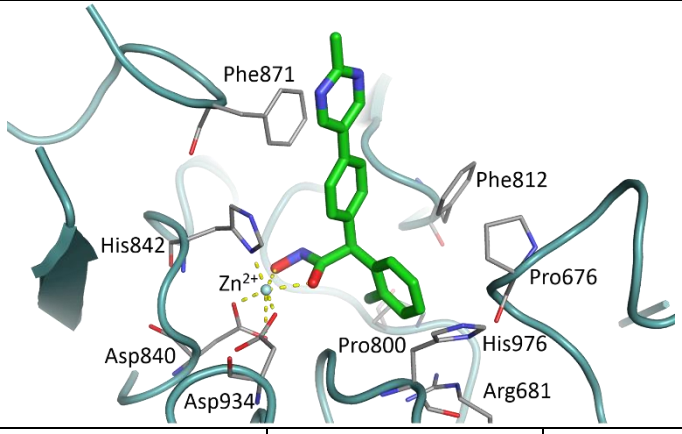

	HDAC1	Ac-Arg-Gly-Lys(Ac)	>50	39.7

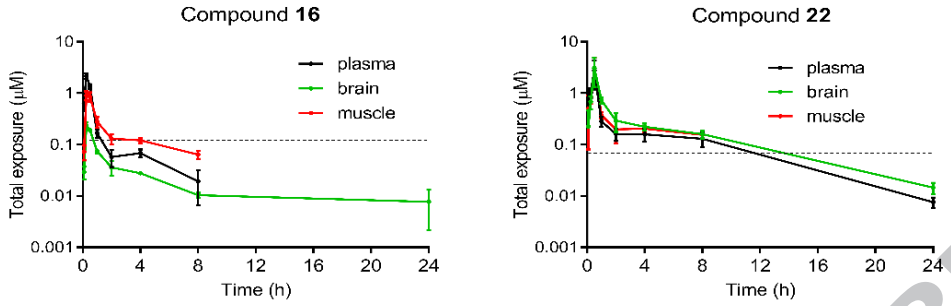

	HDAC2	Ac-Arg-Gly-Lys(Ac)	>50	>50
	HDAC3	Boc Lys(Ac)	25.1	25.8
	HDAC8	Boc Lys(TFA)	6.7	9.1
	HDAC6	Boc Lys(Ac)	6.1	6.2
Cell IC_{50} (µM) [a]	Class IIa (Jurkat)	Boc Lys(TFA)	0.121	0.069
	Class I / IIb Jurkat	Boc Lys(Ac)	>50	>50
	Class I (A549)	H4K12	NT	>30
	Class IIb (A549)	α-Tubulin	NT	17
hERG (IonWorks) - IC_{50} (µM) (max % inh)			>10 (14)	>100 (30)
CYP P450 inhibition (µM)			All > 50	All >50; except 3A4 >35
PPB[b] (% unbound)			11	4.1
Brain tissue binding (% unbound)			12	0.5

[a]Geometric mean of at least three experiments conducted in duplicate; standard deviations are <25% of the mean. [b] Plasma protein binding. NT – not tested.

Figure 3. Total exposure in plasma, brain and muscle matrices for compounds **16** and **22** following a single 10 mg/kg oral gavage to C57/BL6 mice. Data is plotted as mean ± SD (n = 3 per time point). Dashed line indicates class IIa cellular IC_{50} for each compound.

In subsequent oral dose escalation studies, both compounds demonstrated a dose proportional increase in exposure in both plasma and brain matrices (**Figure 4**, **Tables S5** and **S6**). Compound **22** showed the most favorable PK profile, with an approximate 9-fold increase in brain AUC_{norm} compared to compound **16**, and total exposure in both plasma and brain exceeding cellular class IIa HDAC IC_{50} for ~8 h with doses ≥30 mg/kg. Estimations of unbound exposure of **22** in plasma suggested that (steady state) estimations of unbound drug exceeded IC_{50} for ~ 4 h at the 100 mg/kg *po* dose; however, in the brain, the highest estimated unbound exposure (C_{max} following 100 mg/kg oral dose) was equivalent to class IIa cellular IC_{35} (35 nM), suggesting that either a higher dose level or an alternative route of administration may need to be contemplated for effective class IIa HDAC target engagement in the mouse CNS, as unbound exposure may be a better predictor of activity than total exposure levels [23-25]. In this study, the relationship of effective class IIa HDAC inhibition *in vivo* to either total or unbound exposure levels of the compounds have not been determined: class IIa HDAC target engagement in the CNS is notoriously difficult to empirically determine, as no endogenous catalytic site substrate has been definitively determined [1, 2, 5] precluding any straightforward CNS pharmacokinetic–pharmacodynamic evaluation. From evaluation of the HDAC4 binding kinetics for compound **22** (**Table S1**), *in vitro* dissociation half-life of binding to HDAC4, as an indicator of drug-target residence times, was ~3 minutes, suggesting that effective target engagement *in vivo* will likely be driven overwhelmingly by the pharmacokinetic properties of the compound [26].

Figure 4. **Single dose escalation of compounds 16 and 22 in C57/BL6 mice**. Plasma (**A-B**), and brain (**C-D**) exposure of **16** (**A, C**) and **22** (**B, D**) following a single oral gavage at 10 mg/kg (open black circles), 30 mg/kg (open blue circles) or 100 mg/kg (open green circles). Left axis indicates the measured total exposure. Right axis indicates the estimated free (unbound) exposure based on f_u values determined in relevant matrix *in vitro*. Red arrowheads indicate the cellular class IIa HDAC IC_{50} value determined *in vitro*. Data is plotted as mean ± SD (n = 3 per time point).

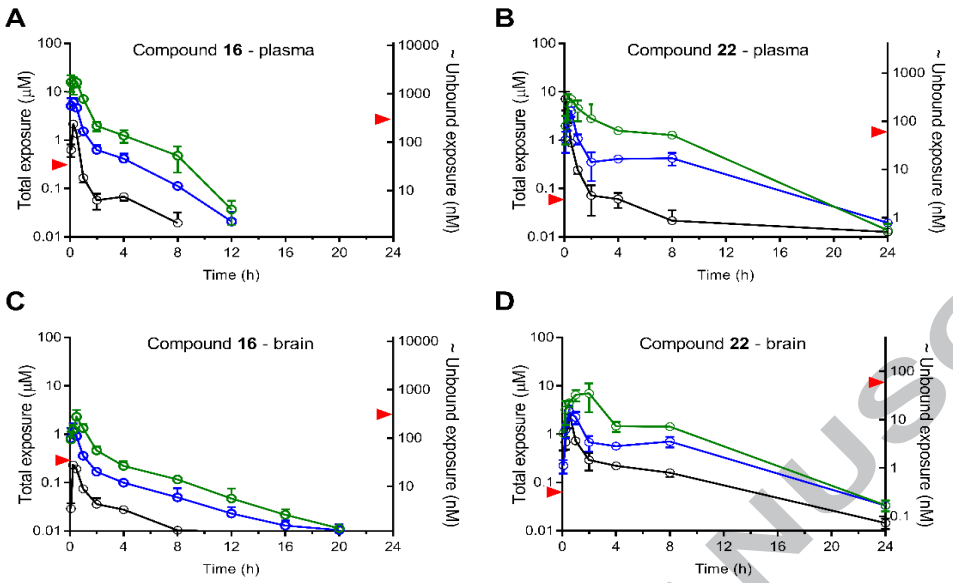

Lastly, given our interest in evaluating this compound for therapeutic potential in Huntington's disease models, tolerability towards repeated dosing with compound **22** was conducted in R6/2 mice [27], a transgenic mouse model of HD, and WT littermates. Mice were dosed orally *b.i.d.* with **22** at 10, 30 or 100 mg/kg or vehicle for 15 days.

Compound **22** was well-tolerated and showed no significant effect on passive observations, responses to manipulations, body weight, or body temperature. However, activity of the compound on measures of open field activity (see Supplementary Methods) were noted in both WT and R6/2 mice: compared to vehicle control, compound **22** (30 and 100 mg/kg) caused a significant increase in open field measures of total and center distance in WT mice ($p<0.05$) and in total and center rearing in both WT and R6/2 mice ($p<0.05$). Average velocity was unchanged. Given the very clean profile of this compound and the central exposure levels empirically determined at these doses, we tentatively conclude that these effects are likely mediated by class IIa HDAC inhibition.

In conclusion, we have optimized the *in vitro* HDAC class IIa selectivity and metabolic stability properties of a series of benzhydryl hydroxamic acid HDAC class IIa inhibitors. This led to the identification of compound **22** from this series (also known as CHDI-390576), whose PK properties make it suitable to evaluate the effect of class IIa inhibition in an *in vivo* setting, and to further explore the potential therapeutic effect of class IIa HDAC catalytic site occupancy in a number of neurodegenerative and oncology indications.

Acknowledgments

The authors would like to thank Mark Sandle, Simon Yau and Paul Bond for analytical support, Saretius for conducting the in-life phase of the PK studies, and the ADME team at BioFocus for undertaking *in vitro* ADME studies and bioanalysis.

Supplementary Material

Supplemental Tables (Table S1- Table S7).

Supplemental Methods and Materials.

References

1. Bertos NR, Wang AH, Yang XJ: **Class II histone deacetylases: structure, function, and regulation**. *Biochem Cell Biol* 2001, **79**(3):243-252.

2. Fitzsimons HL: **The class IIa histone deacetylase HDAC4 and neuronal function: Nuclear nuisance and cytoplasmic stalwart?** *Neurobiol Learn Mem* 2015, **123**:149-158.
3. Mielcarek M, Zielonka D, Carnemolla A, Marcinkowski JT, Guidez F: **HDAC4 as a potential therapeutic target in neurodegenerative diseases: a summary of recent achievements**. *Front Cell Neurosci* 2015, **9**:42.
4. Di Giorgio E, Brancolini C: **Regulation of class IIa HDAC activities: it is not only matter of subcellular localization**. *Epigenomics* 2016, **8**(2):251-269.
5. Lahm A, Paolini C, Pallaoro M, Nardi MC, Jones P, Neddermann P, Sambucini S, Bottomley MJ, Lo Surdo P, Carfi A *et al*: **Unraveling the hidden catalytic activity of vertebrate class IIa histone deacetylases**. *Proc Natl Acad Sci U S A* 2007, **104**(44):17335-17340.
6. Wright LH, Menick DR: **A class of their own: exploring the nondeacetylase roles of class IIa HDACs in cardiovascular disease**. *Am J Physiol Heart Circ Physiol* 2016, **311**(1):H199-206.
7. McGee SL, Hargreaves M: **Histone modifications and skeletal muscle metabolic gene expression**. *Clin Exp Pharmacol Physiol* 2010, **37**(3):392-396.
8. Bai G, Wei D, Zou S, Ren K, Dubner R: **Inhibition of class II histone deacetylases in the spinal cord attenuates inflammatory hyperalgesia**. *Mol Pain* 2010, **6**:51.
9. Kee HJ, Kook H: **Roles and targets of class I and IIa histone deacetylases in cardiac hypertrophy**. *J Biomed Biotechnol* 2011, **2011**:928326.
10. Guerriero JL, Sotayo A, Ponichtera HE, Castrillon JA, Pourzia AL, Schad S, Johnson SF, Carrasco RD, Lazo S, Bronson RT *et al*: **Class IIa HDAC inhibition reduces breast tumours and metastases through anti-tumour macrophages**. *Nature* 2017, **543**(7645):428-432.
11. Abend A, Kehat I: **Histone deacetylases as therapeutic targets--from cancer to cardiac disease**. *Pharmacol Ther* 2015, **147**:55-62.
12. Choi MC, Cohen TJ, Barrientos T, Wang B, Li M, Simmons BJ, Yang JS, Cox GA, Zhao Y, Yao TP: **A direct HDAC4-MAP kinase crosstalk activates muscle atrophy program**. *Mol Cell* 2012, **47**(1):122-132.
13. Mielcarek M, Toczek M, Smeets CJ, Franklin SA, Bondulich MK, Jolinon N, Muller T, Ahmed M, Dick JR, Piotrowska I *et al*: **HDAC4-myogenin axis as an important marker of HD-related skeletal muscle atrophy**. *PLoS Genet* 2015, **11**(3):e1005021.
14. Valsecchi V, Boido M, De Amicis E, Piras A, Vercelli A: **Expression of Muscle-Specific MiRNA 206 in the Progression of Disease in a Murine SMA Model**. *PLoS One* 2015, **10**(6):e0128560.
15. Bruneteau G, Simonet T, Bauche S, Mandjee N, Malfatti E, Girard E, Tanguy ML, Behin A, Khiami F, Sariali E *et al*: **Muscle histone deacetylase 4 upregulation in amyotrophic lateral sclerosis: potential role in reinnervation ability and disease progression**. *Brain* 2013, **136**(Pt 8):2359-2368.
16. Di Pietro L, Baranzini M, Berardinelli MG, Lattanzi W, Monforte M, Tasca G, Conte A, Logroscino G, Michetti F, Ricci E *et al*: **Potential therapeutic targets for ALS: MIR206, MIR208b and MIR499 are modulated during disease progression in the skeletal muscle of patients**. *Sci Rep* 2017, **7**(1):9538.
17. Williams AH, Valdez G, Moresi V, Qi X, McAnally J, Elliott JL, Bassel-Duby R, Sanes JR, Olson EN: **MicroRNA-206 delays ALS progression and promotes regeneration of neuromuscular synapses in mice**. *Science* 2009, **326**(5959):1549-1554.
18. Mielcarek M, Landles C, Weiss A, Bradaia A, Seredenina T, Inuabasi L, Osborne GF, Wadel K, Touller C, Butler R *et al*: **HDAC4 reduction: a novel therapeutic strategy to target cytoplasmic huntingtin and ameliorate neurodegeneration**. *PLoS Biol* 2013, **11**(11):e1001717.
19. Burli RW, Luckhurst CA, Aziz O, Matthews KL, Yates D, Lyons KA, Beconi M, McAllister G, Breccia P, Stott AJ *et al*: **Design, synthesis, and biological evaluation of potent and selective class IIa histone deacetylase (HDAC) inhibitors as a potential therapy for Huntington's disease**. *J Med Chem* 2013, **56**(24):9934-9954.
20. Luckhurst CA, Breccia P, Stott AJ, Aziz O, Birch HL, Burli RW, Hughes SJ, Jarvis RE, Lamers M, Leonard PM *et al*: **Potent, Selective, and CNS-Penetrant Tetrasubstituted Cyclopropane class IIa Histone Deacetylase (HDAC) Inhibitors**. *ACS Med Chem Lett* 2016, **7**(1):34-39.
21. Tessier P, Smil DV, Wahhab A, Leit S, Rahil J, Li Z, Deziel R, Besterman JM: **Diphenylmethylene hydroxamic acids as selective class IIa histone deacetylase inhibitors**. *Bioorg Med Chem Lett* 2009, **19**(19):5684-5688.
22. Mahar Doan KM, Humphreys JE, Webster LO, Wring SA, Shampine LJ, Serabjit-Singh CJ, Adkison KK, Polli JW: **Passive permeability and P-glycoprotein-mediated efflux differentiate central nervous system (CNS) and non-CNS marketed drugs**. *J Pharmacol Exp Ther* 2002, **303**(3):1029-1037.
23. Heffron TP: **Challenges of developing small molecule kinase inhibitors for brain tumors and the need for emphasis on free drug levels**. *Neuro Oncol* 2017.
24. Rankovic Z: **CNS drug design: balancing physicochemical properties for optimal brain exposure**. *J Med Chem* 2015, **58**(6):2584-2608.
25. Reichel A: **Addressing central nervous system (CNS) penetration in drug discovery: basics and implications of the evolving new concept**. *Chem Biodivers* 2009, **6**(11):2030-2049.
26. Dahl G, Akerud T: **Pharmacokinetics and the drug-target residence time concept**. *Drug Discov Today* 2013, **18**(15-16):697-707.
27. Mangiarini L, Sathasivam K, Seller M, Cozens B, Harper A, Hetherington C, Lawton M, Trottier Y, Lehrach H, Davies SW, Bates GP (1996) **Exon 1 of the HD gene with an expanded CAG repeat is sufficient to cause a progressive neurological phenotype in transgenic mice**. Cell 1996, **87**(3):493-506.

Twenty hydroxamic acid inhibitors of class IIa histone deacetylases were synthesized
Inhibitor **22** (CHDI-390576) was selective over class I and IIb histone deacetylases
Inhibitor **22** can reach high exposure levels in mouse plasma, muscle and brain

Graphical Abstract

To create your abstract, type over the instructions in the template box below.
Fonts or abstract dimensions should not be changed or altered.

Development and characterization of a CNS-penetrant benzhydryl hydroxamic acid class IIa histone deacetylase inhibitor

Leave this area blank

Christopher A. Luckhurst, Omar Aziz, Vahri Beaumont, Roland W. Bürli, Perla Breccia, Michel C. Maillard*, Alan F. Haughan, Marieke Lamers, Phil Leonard, Kim L. Matthews, Gilles Raphy, Andrew J. Stott, Ignacio Munoz-Sanjuan, Beth Thomas, Michael Wall, Grant Wishart, Dawn Yates and Celia Dominguez.